How well does ramped thermal oxidation quantify the age distribution of soil carbon? Assessing thermal stability of physically and chemically fractionated soil organic matter

Shane W. Stoner[1,2], Marion Schrumpf[1], Alison Hoyt[3], Carlos A. Sierra[1,4], Sebastian Doetterl[2], Valier Galy[5], Susan Trumbore[1]

[1]Biogeochemical Processes Department, Max Planck Institute for Biogeochemistry, Jena, 07745, Germany

[2]Department of Environmental Systems Science, ETH Zürich, Zürich, 8092, Switzerland

[3]Earth System Science, Stanford University, Stanford, 94305, USA

[4]Department of Ecology, Swedish University of Agricultural Sciences, Uppsala, SE-750 07, Sweden

[5]Woods Hole Oceanographic Institution, Woods Hole, 02543, USA

Correspondence to: Shane W. Stoner (sstoner@bgc-jena.mpg.de)

Abstract

Carbon (C) in soils persists on a range of timescales depending on physical, chemical and biological processes that interact with soil organic matter (SOM) and affect its rate of decomposition. Together these processes determine the age distribution of soil C. Most attempts to measure this age distribution have relied on operationally defined fractions using properties like density, aggregate stability, solubility, or chemical reactivity. Recently, thermal fractionation, which relies on the activation energy needed to combust SOM, has shown promise for separating young from old C by applying increasing heat to decompose SOM. Here, we investigated radiocarbon (^{14}C) and ^{13}C of C released during thermal fractionation to link activation energy to the age distribution of C in bulk soil and components previously separated by density and chemical properties. While physically and chemically isolated fractions had very distinct mean ^{14}C values, they contributed C across the full temperature range during thermal analysis. Thus, each thermal fraction collected during combustion of bulk soil integrates contributions from younger and older C derived from components having different physical and chemical properties but the same activation energy. Bulk soil and all density and chemical fractions released progressively older and more ^{13}C-enriched C with increasing activation energy, indicating that each operationally defined fraction itself was not homogeneous but contained a mix of C with different ages and degrees of microbial processing. Overall, we found that defining the full age distribution of C in bulk soil is best quantified by first separating particulate C prior to thermal fractionation of mineral-associated SOM. For the Podzol analyzed here, thermal fractions confirmed that ~95% of the mineral-associated organic matter (MOM) had a relatively narrow ^{14}C distribution, while 5% was very low in ^{14}C and likely reflected C from the < 2mm parent shale material in the soil matrix. After first removing particulate C using density or size separation, thermal fractionation can provide a rapid technique to study the age structure of MOM and how it is influenced by different OM-mineral interactions.

1 Introduction

Soil organic matter (SOM) consists of a complex and diverse collection of organic molecules containing C that can persist in soil for timescales ranging from hours to millennia (Schuur et al., 2016). Plant tissue chemistry, soil environmental conditions, soil mineral characteristics, physical aggregation, and microbial communities have all been demonstrated to impact the stability of SOM (Lehmann and Kleber, 2015; Basile-Doelsch et al., 2020; Kleber et al., 2021). These factors collectively influence the age of carbon (C) in SOM and the age of C in microbial respiration, making it challenging to link the timescales of OM stabilization and destabilization to the various mechanisms that allow C to persist in soils.

Measurement of soil radiocarbon (^{14}C) has been used for decades to describe mean SOM ages. However, the mean ^{14}C values measured on bulk SOM integrate different pools and stabilization mechanisms and thereby obscure critical information on the distribution of SOM age. By combining timescales from years to millennia, interpretation of bulk ^{14}C measurements is made more difficult due to integration of ^{14}C from both natural sources affected by radioactive decay (natural ^{14}C, integrating multiple centuries to millennia) and ^{14}C produced by atomic weapons ("bomb" ^{14}C) that reflect short-term cycling (annual to century) (Trumbore, 2000; Baisden and Canessa, 2013). Disentangling these signals is complex and requires the integration of ^{14}C data with models to estimate SOM transit times and ages (Sierra et al., 2018; Metzler et al., 2018).

In an effort to better describe the distribution of age and cycling rates in bulk SOM, a number of physical and chemical fractionation methods have been developed to elucidate how the bulk ^{14}C can be broken into pools with different amounts of ^{14}C depending on physical or chemical characteristics (Trumbore et al., 1990; Paul et al., 1997; Castanha et al., 2008; Sollins et al., 2009; Lavallee et al., 2020). In particular, density fractionation, a method that separates SOM associated with denser minerals from low-density 'free' particulate organic matter (FPOM), has demonstrated success in distinguishing faster (low density) from slower (mineral associated) cycling C (Gregorich et al., 2006; Cotrufo et al., 2019; Heckman et al., 2022). However, mineral-associated organic matter (MOM) fractions themselves have been shown by many studies to be comprised of both faster and slower cycling C as evidenced by the change in ^{14}C content after chemical extraction or oxidation (examples include Anderson and Paul, 1984; Balesdent, 1987; Trumbore and Zheng, 1996; Jagadamma et al., 2010; Schrumpf et al., 2021) or from tracking bomb ^{14}C into mineral fractions (examples include Trumbore, 1993; Torn et al., 1997; von Lützow et al., 2007, and more recently Schrumpf et al., 2013; Rasmussen et al., 2018; Heckman et al., 2018). Despite their widespread use and demonstrated utility for separating organic C by age as well as physical and chemical properties, most fractionation methods consume significant laboratory time and resources (Lavallee et al., 2020; Heckman et al., 2022). Further, some treatments, such as dense sodium polytungstate solution, remove C that cannot be easily recovered or analyzed for C or ^{14}C content, meaning that the isotopic signature of removed C must be solved using mass balance constraints.

70 Ramped pyrolysis/oxidation (RPO), or thermal fractionation, is a relatively new method to functionally fractionate OM in sediments and soils (Rosenheim et al., 2008; Plante et al., 2013; Hemingway et al., 2017). This process

72 applies increasing temperature of thermal decomposition as a proxy for the activation energy (E_a) required to oxidize C, with the assumption that this provides a comparable measure of its resistance to decomposition in the soil

74 environment. The result is a reproducible profile of CO_2 released as a function of increasing temperature (thermogram), from which E_a distributions can be calculated (Hemingway et al., 2017). By collecting the CO_2

76 released over specified intervals as temperatures are continuously increased, "pools" of C with distinct thermal stability can be isolated, collected, and analyzed isotopically (Rosenheim and Galy, 2012). Because all C is released

78 as CO_2, it is possible to characterize all of the C in a sample rather than inferring losses from analysis of the residual material. A further advantage of such "thermal fractionation" is that it can be compared with pyrolysis-GC/MS of

80 SOM to evaluate how the chemistry of combusted SOM also changes with E_a. Previous studies have shown that the breakdown of lipids and polysaccharides releases C at lower temperatures, while thermal decomposition of phenolic

82 and aromatic compounds dominate at higher temperatures (Quénéa et al., 2006; Grandy et al., 2009; Sanderman and Grandy, 2020). Thus, thermal fractionation has the potential to define the ^{14}C (age) distribution of organic C and

84 relate that to the E_a and chemistry of the OM in a soil sample.

86 Several studies have investigated soils using oxidative thermal fractionation (Plante et al., 2013; Grant et al., 2019; Hemingway et al., 2019). Compared to sediments, where these methods have been more widely applied, soil

88 thermograms release a greater proportion of the total C over a narrower temperature range and have lower variation in age across thermal fractions (Hemingway et al., 2019). This may reflect a broader set of OM sources in sediments

90 that can include eroded soil containing very old and highly processed C as well as fresh material from aquatic organisms.

92

   Typically, C released from both sediments and soils by thermal oxidation also increases in age with temperature of

94 combustion, i.e., E_a, confirming linkages between SOM persistence and the mechanisms of C stabilization (Plante et al., 2011; González-Pérez et al., 2012). However, different SOM stabilization mechanisms or local environments

96 can complicate the interpretation of E_a-age relationships; for example, the same chemical compound sorbed to different mineral substrates can have very different activation energies (Feng and Simpson, 2008). Thermal

98 oxidation of OM not associated with minerals, such as dissolved organic C (DOC), oxidizes at narrow but relatively high temperature ranges, possibly contributing young C at high temperatures that would be mixed with C released

100 from mineral fractions at the same temperature (Grant et al., 2019; Hemingway et al., 2019). Given the wide range of ^{14}C ages measured in various physical and chemical fractions, and the potential for recycling of C in soils through

102 microbial processing, we expect some range of C age within each bulk soil thermal fraction.

104 Here, we apply oxidative thermal fractionation to SOM previously separated using physical (density) and chemical (extraction and oxidation) methods. Using mass balance approaches, we describe the contribution of each fraction

106 to bulk soil thermograms and ^{14}C signatures. We also present thermal fractionation results using a commercially

available instrument only recently applied to characterize SOM thermal stability distributions (Natali et al., 2020; Rennert and Herrmann, 2020, 2022). Our goals were to determine (1) the degree to which the physically and chemically separated fractions represent mixtures of OM with different activation energies and ^{14}C distributions; (2) to determine the ^{14}C distribution of C contained in physically or chemically separated fractions; (3) to assess the viability of thermal fractionation as an alternative to more time intensive lab methods in determining the ^{14}C distribution of SOM.

2 Methods

2.1 Site description and density fractionation

Soil material used in this study was sampled from a Podzol developed on granitic parent material under spruce forest in central Germany (Schrumpf et al., 2013, 2021). This soil was selected because it was already known to have large differences in ^{14}C content between density fractions (Schrumpf et al., 2021) and because of strong depth-dependent differences in stabilization processes in Podzol A and B horizons (De Coninck, 1980). Surface (0-10 cm) and subsoil (30-50 cm) samples were subjected to laboratory fractionations described in detail by Schrumpf et al. (2013). Briefly, soils first underwent density separation using dense sodium polytungstate solution (SPT) (1.6 g/cm^3). Suspended OM was separated from denser material that did not float using centrifugation. The floating free particulate OM (FPOM) fraction was collected and rinsed to remove remaining SPT solution. The sinking fraction was dispersed again in 1.6 g cm^{-3} solution and sonicated to disrupt aggregates, then centrifuged. After centrifugation, floating material from the supernatant was collected, rinsed, and designated as occluded particulate organic matter (OPOM). The remaining dense material in the sediment was repeatedly rinsed to remove SPT solution and is designated mineral associated organic matter (MOM).

2.2 Chemical fractionation

Two chemical fractionations were performed in parallel on the MOM fraction, as described by Schrumpf et al. (2021). The first subsample was extracted with NaF-NaOH to solubilize and remove all potentially de-sorbable SOM complexed with minerals through pH increase and competition with OH- and F- anions (Kaiser et al., 2007; Mikutta and Kaiser, 2011). Briefly, 125 mL of a NaF-NaOH solution was added to 25g MOM material, agitated overnight, and centrifuged. The supernatant was extracted, and an additional 125 mL of NaF-NaOH was added to repeat this process four times in total. Then, each extraction was filtered through glass fiber filters and combined. The remaining soil material was washed with deionized water and freeze-dried.

The second chemically treated MOM underwent strong oxidation in heated hydrogen peroxide (H_2O_2) to isolate the most resistant and oldest OM (Helfrich et al., 2007; Jagadamma et al., 2010). In this procedure, 60 mL H_2O_2 was added to a mixture of 2 g MOM and 20 mL deionized water. Samples were then heated and periodically stirred in a 50˚C water bath for a total of 120 hours. Samples were then centrifuged, washed with deionized water, freeze dried, and homogenized with a ceramic ball mill.

2.3 Thermal fractionation and method development

144 Oxidative thermal fractionation of bulk SOM and physically and chemically separated fractions was performed using an Elementar soliTOC Cube carbon analyzer. Samples were not analyzed under pyrolytic conditions, as pyrolysis

146 can produce charring artifacts, and ^{14}C distributions have been shown to be comparable between operational modes (Williams et al., 2014; Grant et al., 2019). The design of the instrument used is very similar to those used in previous

148 thermal fractionation publications (Rosenheim and Galy, 2012; Bianchi et al., 2015). Primarily, it consists of two ovens in sequence, a mechanical arm to hold and manipulate the sample container, and a non-dispersive infrared

150 analyzer (NDIR) to measure the CO_2 concentration in the gas exiting the ovens. The sample is introduced to the first oven, which is heated at a constant rate under a constant flow of carrier gas supplied through the sampler arm (78%

152 N_2, 22% O_2). The second oven contains a Pt catalyst held at 800˚C that ensures all C released from the sample is oxidized to CO_2. The carrier gas then passes through a glass tube filled with brass wire at 20˚C to remove HCl from

154 acidified samples (note that no samples were acidified in this experiment) followed by a glass tube containing magnesium perchlorate to remove water vapor. Finally, CO_2 concentration in the gas mixture is measured by the

156 NDIR (DIN 19539).

158 Several additional procedures were required to adapt use of the commercial device for collection of C released by thermal fractionation. Due to the relatively large sample size (> 1g of dried soil or fraction) required to collect small

160 thermal fractions with sufficient C for radiocarbon measurement, and the high flow rate of carrier gas in this instrument, samples with high C content (such as standards or FPOM/OPOM fractions) were diluted to ~2% (by

162 weight) C with pre-combusted sand (1000˚C for 10 hours) to prevent ignition and charring during heating. An artificial soil standard was analyzed with different sand dilutions to ensure that thermograms were not altered by

164 dilution with sand (Fig. S1). Further, the sample oven was designed for rapid heating (up to 110˚C min^{-1}), and temperatures were observed to be less stable at slower heating rates. To reduce the cycles of on/off oven cycling

166 while ensuring thermogram consistency (with sand dilution), samples were heated at 15˚C per minute.

168 To collect CO_2 for isotope analysis, a custom collection manifold was attached to the instrument outflow port (Figs. S2-S4). The manifold consists of parallel glass CO_2 traps submerged in LN_2 under vacuum. Exhaust gas released

170 within a desired temperature range (thermal fraction) flows through a cold trap until the desired upper temperature is reached. Then, the trap is closed and the next opened to collect the next CO_2 fraction. This process is repeated for

172 each thermal fraction (F1 (first thermal fraction) – F*max* (highest temperature thermal fraction), see Appendix tables 1 and 2). A vacuum pump together with a capillary restriction upstream of the manifold was used to reduce the

174 overall pressure in the manifold system to < 6 mbar to improve cryotrapping efficiency and to prevent condensation of O_2 in the LN_2 traps.

176

Traps with CO_2 samples were subsequently transferred to a vacuum line where the CO_2 was further purified (see

178 below) and measured volumetrically for comparison (calibration) of the NDIR CO_2 analysis. An aliquot was taken for analysis of $\delta^{13}C$ using a modified gasbench inlet to a continuous flow IRMS (Wendeberg et al., 2013). In addition

180   to CO_2, we noticed that nitrogen oxide gasses (including N_2O_3, which is dark blue when frozen) were visibly trapped. These gasses are produced by the reaction of N_2 and O_2 at high temperatures. As these, as well as S oxides that also

182   freeze with CO_2 at liquid nitrogen temperatures, can cause graphitization failure, we used an additional purification procedure to remove them. An amount of sample CO_2 representing approximately 0.5 mg C was transferred

184   cryogenically and then sealed under vacuum in a pre-combusted borosilicate tube containing ~50 mg CuO and ~10 mg Ag (Hemingway et al., 2017) and baked at 525˚C for one hour. Purified CO_2 released after breaking this tube

186   was graphitized using zinc reduction (Xu et al., 2007) and measured at the Keck AMS lab at University of California Irvine. Resulting radiocarbon data are expressed as Fraction Modern (Fm).

188

Thermograms and activation energy (E_a) were analyzed using the open-source "rampedpyrox" Python package

190   (Hemingway, 2017; Hemingway et al., 2017). For each thermogram, a distributed E_a model derived from time-temperature C-release data is solved inversely to produce a continuous distribution of E_a (in kJ mol^{-1}). It assumes a

192   finite set of n components (thermal fractions, in order of increasing temperature, referred to as F1 - F*max*, where F*max* is thermal F$_n$, the highest temperature range collected (Appendix tables 1 and 2) in superposition to construct

194   the bulk soil E distribution. Each of these components can thus be mathematically assigned a mean E_a (μE) and standard deviation (σE). Here, standard deviation describes the variance of distribution of E, or the heterogeneity of

196   the bonding environment, within a thermal fraction or sample, rather than data variance. Thus, direct comparisons can be made between E distribution within a thermal fraction and its isotopic composition. However, it should be

198   noted that such E_a descriptors derived from thermograms are not necessarily comparable to other methods of measuring E_a (Feng and Simpson, 2008; Hemingway et al., 2019).

200

3 Results

202   We describe data on SOM decomposition as a function of temperature, modeled E_a, and isotopic signatures of thermal fractions within and between density and chemical fractions and compare these to thermal fractionation of

204   the bulk soil. To our knowledge, this was the first thermal fractionation procedure performed using a commercial C analyzer. Results on the performance and reliability of this setup to demonstrate the viability of this method for

206   future researchers are presented in Supplemental Text 1.

208 **Table 1:** Summary information of bulk soil and fraction thermal stability and isotopic compositions, including activation energy indices. Fm = Fraction Modern [14]C

Depth	Fraction	Fraction Percent of Total C	μE (kJ mol^{-1})	σE (kJ mol^{-1})	Whole Fraction Fm	Max Thermal Fm[a]	Min Thermal Fm[a]
0-10 cm	Bulk Soil	-	134.1	14.2	0.997	1.048	0.751
0-10 cm	FPOM	8.7	133.5	15.3	1.080	1.102	1.067
0-10 cm	OPOM	6.2	135.3	14.0	0.992	1.040	0.968
0-10 cm	MOM	85.1	133.7	15.8	0.985	1.037	0.728
0-10 cm	NaF Res.	28.8	137.8	18.2	0.912	0.959	0.761
0-10 cm	H$_2$O$_2$ Res.	13.5	136.3	12.8	0.859	0.868	0.781
30-50 cm	Bulk Soil	-	138.7	14.0	0.824	0.854	0.323
30-50 cm	FPOM	15.6	141.8	15.9	1.087	1.085	1.064
30-50 cm	OPOM	8.2	144.3	14.7	0.847	0.869	0.822
30-50 cm	MOM	76.3	137.9	16.1	0.786	0.791	0.230 [b]
30-50 cm	NaF Res.	29.9	137.9	24.7	0.713	0.798	0.562
30-50 cm	H$_2$O$_2$ Res.	15.5	141.2	17.7	0.628	0.753	0.414

210

[a]: Maximum and minimum ^{14}C content collected via thermal fractionation within the sample

212 [b]: Value calculated by mass balance, +/- 0.02 Fm

3.1 Thermograms and activation energy of physically and chemically fractionated organic matter

214   We compared the thermograms and the isotopic (^{14}C and ^{13}C) signatures of CO_2 released as a function of temperature for each physical and chemical fraction individually, then compared the summed contribution of each

216   physical/chemical fraction to the bulk soil (for density fractions) or MOM (for chemical fractions) to assess (1) the behavior of each of the different fractions and (2) how much each fraction contributes to the bulk thermogram at

218   different temperature intervals.

220   All density and chemical fractions and bulk soil released 90-98% of their total C between 150 and 500˚C. No fraction had a unique thermal signature (Figures 1a, 1b), and the thermograms mostly overlapped, with some C released

222   across the whole temperature range of combustion. However, differences were observed among density fraction thermograms. For particulate fractions (FPOM and OPOM), C release displayed one or two muted peaks and most

224   of the C was oxidized between 250 and 450˚C. MOM and chemical residues released most of their C between 250 and 350°C, but also released more C at temperatures >500°C compared to FPOM and OPOM fractions. Since most

226   bulk soil C is in the MOM fraction (Table 1), thermograms for the bulk soil resemble those of the MOM fractions in both depths (Fig. 1a).

228

Mean activation energy (μE) estimated from thermograms of bulk soil and fractions ranged from 133.5 to 137.8 kJ

230   mol^{-1} in surface soil and 137.9 to 144.3 kJ mol^{-1} in subsoil (Table 1, Appendix figs. 1 & 2, Appendix tables 1 & 2). Between depths, μE was greater in subsoil than surface soil on average by 5.2 kJ mol^{-1} ($p = 0.01$, paired t-test) for

232   all samples except NaF extraction residues, which showed no difference. In subsoil, particulate fractions FPOM and OPOM μE values were ~3-6 kJ mol^{-1} greater than bulk soil and MOM but showed little difference in surface soils.

234   Standard deviation of E (σE), a metric of bond strength heterogeneity, only varied with depth among chemical fraction residues which were ~5-6 kJ mol^{-1} greater in subsoil, suggesting greater diversity of bonds in the subsoil

236   fractions (Hemingway et al. 2017). Thus, despite large differences in the chemistry and relationship to mineral surfaces, the E_a range was similar across all chemical and physical fractions. It is puzzling that NaF and H_2O_2

238   residues had lower activation energies than might be expected, given that they represent the most "recalcitrant" C resistant to harsh chemical treatments.

240
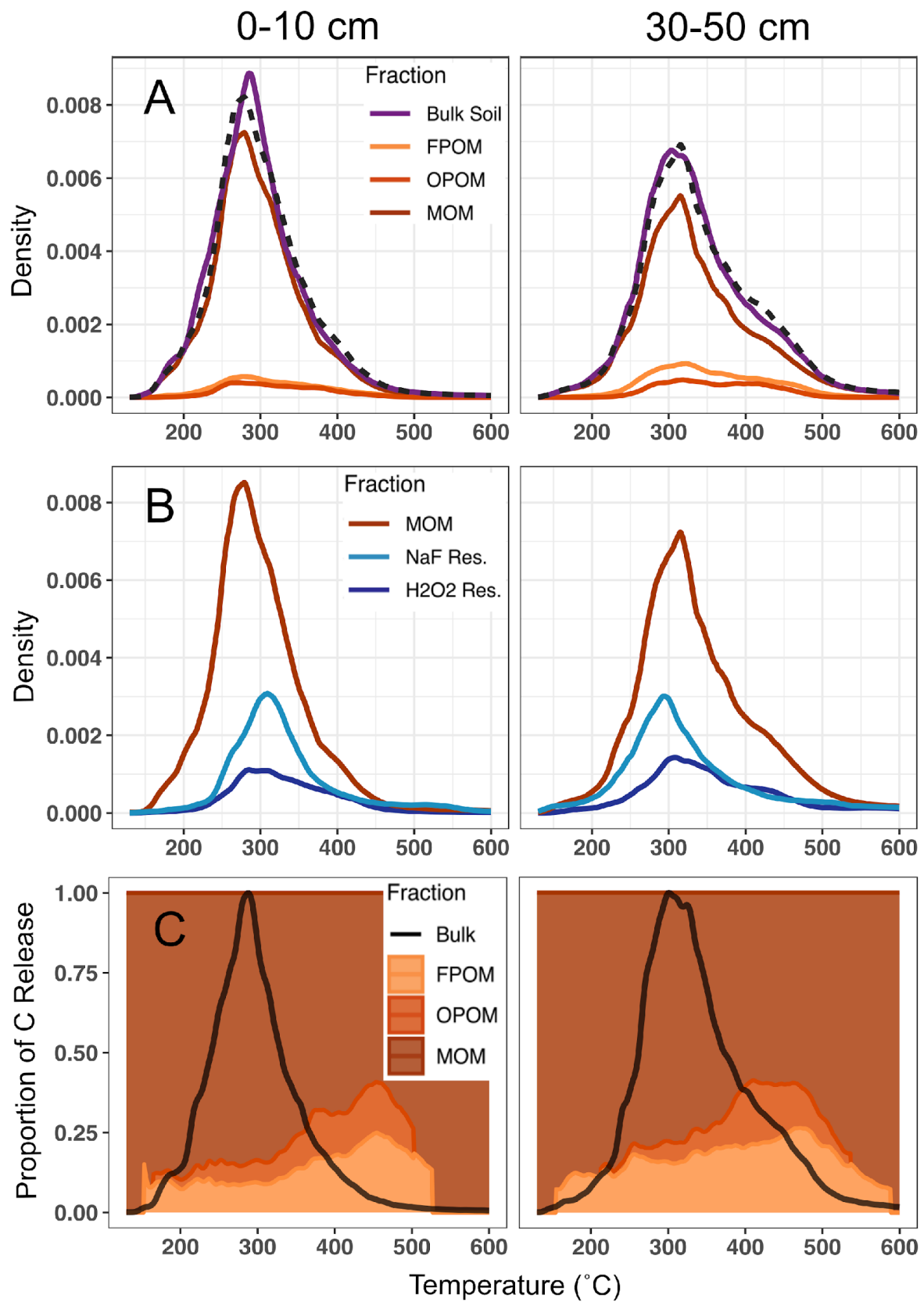
242   **Figure 1:** Relative magnitudes of thermograms, as C released as a function of temperature, with fractions scaled by their relative contribution to the total C in each panel. A: Bulk soil and density fraction thermograms, for 0-10 cm

244   and 30-50 cm, respectively. Density fraction (FPOM, OPOM, MOM) thermograms are scaled to their relative contribution to total bulk soil C (Table 1). Dashed lines represent summed thermograms of the three density

246   fractions. Comparison of summed and bulk thermograms show good agreement and suggest that fractionation procedures do not significantly alter the thermal stability of component fractions. B: Thermograms of MOM and

248   chemical fractionation residues. The difference between MOM and given chemical fraction thermograms represent the thermal profile of C removed by the chemical treatment (NaF-NaOH or H_2O_2). Chemical fraction residue

250   thermograms are scaled to their relative residual C content of the MOM fraction. C: Proportional contribution of density fractions to bulk soil C released across collection temperature range (colored fill). Solid black line represents

252   bulk soil thermogram to highlight total C release from bulk soil at each temperature. Density fractions are cut off when C release is no longer discernible from instrument IR-detector background.

254
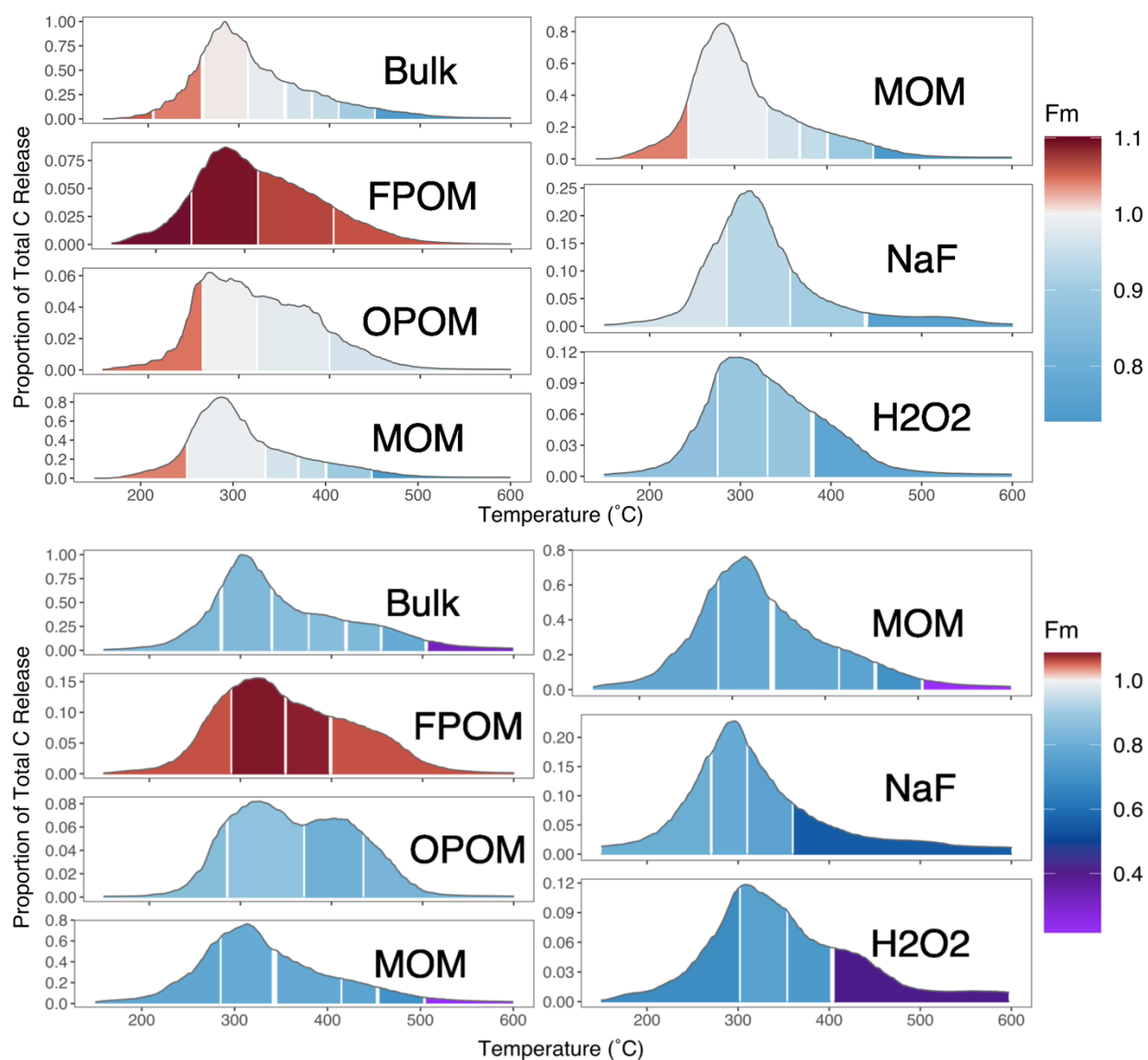
Figure 2: Thermograms with radiocarbon measurements. Top) 0-10 cm, Bottom) 30-50 cm. Left-hand column Y-axis values represent contribution to the total (bulk soil) C. NaF Res. and H2O2 Res. panels are scaled in proportion to their total C contribution to MOM. Color scale indicates the Fraction Modern (Fm) of the C released in each temperature range; the scale is doubled above Fm 1 to emphasize differences between post-bomb [14]C (Fm >1.0) and ^{14}C that has undergone significant radioactive decay (Fm <1).

262
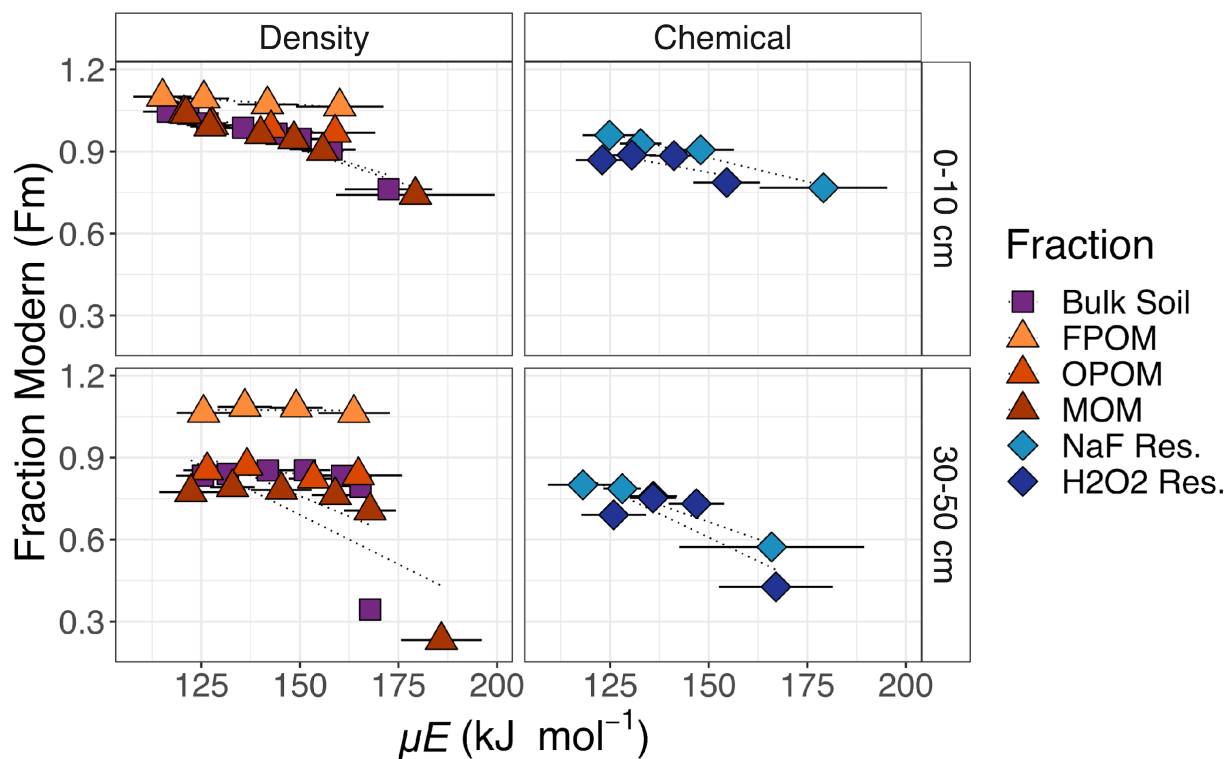
Figure 3: Radiocarbon (Fm) as a function of mean activation energy (μE) for C collected across different temperature

264   intervals from combustion of bulk soil, compared with those of combusted component density and chemical fractions.

Horizontal bars represent σE for each thermal fraction, which indicates the range of activation energies represented

266   by a given thermal fraction.
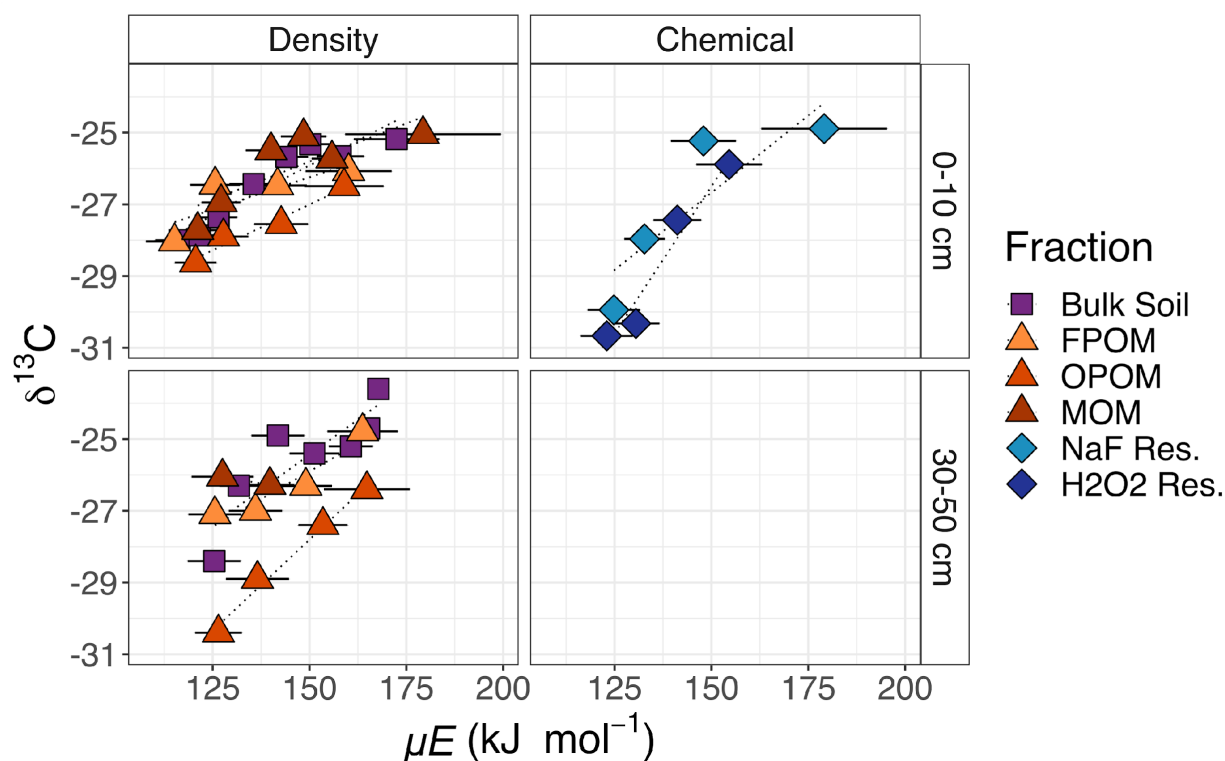
Figure 4: $\delta^{13}C$ measured for each fraction as in Figure 3. Low C content and limited sample material prevented data collection from some fractions (MOM, NaF Res., H_2O_2 Res. in subsoil). Right-hand labels denote depth in cm.

3.2 Radiocarbon

The mean radiocarbon (^{14}C, expressed as Fm) differed for each density or chemical residue fraction (Table 1). For a given soil depth, the FPOM had the highest ^{14}C content, consisting mostly of C fixed since the 1960's (Fm >1.0), while the lowest ^{14}C was in the residue after H_2O_2 treatment of the MOM. The ^{14}C of the bulk soil and each fraction decreased from the 0-10 cm to 30-50 cm depth, and the overall pattern of Fm for the different physical and chemical fractions (FPOM> OPOM> MOM> NaF residue > H_2O_2 residue) remained the same.

Within all fractions, the Fm of released CO_2 stayed similar or declined as the temperature increased (Figure 2; temperatures of combustion are converted to E_a in Figure 3). In both Figures 2 and 3, the large differences in ^{14}C between the FPOM other density and chemical fractions far exceed the range of Fm released across temperatures during combustion of the individual fractions. Indeed, as reported by Schrumpf et al. (2021), much of the combusted C from MOM fractions had very similar ^{14}C signatures (small range of Fm), except for the highest temperature / E_a fractions of MOM and Bulk soil.

For the bulk soil and MOM fraction in the surface sample, and FPOM fractions at both depths, the C oxidized at the lowest temperature had Fm >1, indicating that a portion of the C in the fraction was fixed mostly in the last 60 years. For the FPOM fractions with Fm >1, ^{14}C values are not as simply related to 'age' of the C. For example, the most

recently fixed C could have lower values than the mean, but so could older C if that is a mixture of pre-and post-bomb C. For all samples other than FPOM, the decline in Fm ^{14}C indicates a clear trend of increasing age (decreasing Fm, indicating more time for radioactive decay of ^{14}C) especially at temperatures above that where most C was released (Figure 2). The highest-temperature thermal fractions (Fmax, mostly 450 - 800°C, Appendix tables 1 and 2) of surface bulk soil and MOM were similarly depleted in ^{14}C and much older than any other values measured (Fig. 2).

In subsoils (30-50 cm), bomb ^{14}C was found only in the FPOM fractions, so the decline in ^{14}C with energy was determined mostly by the much lower ^{14}C of C released at high temperatures (Figure 3). All fractions except the NaF Residue (NAF Res.) increased in Fm from the C collected in F1 and F2 (and F3 in bulk soil) temperature ranges (140-375°C), followed by decreases at increasingly higher temperatures. Excluding FPOM and OPOM, all fractions decreased significantly in Fm in Fmax compared to the temperature range previous.

The chemical fractionation residues contained C with lower Fm than the unextracted MOM at all temperature ranges except in the highest temperature range collected. However, the highest temperature fraction collected for the MOM was greater (505 - 750°C), because insufficient C evolved from the chemical fraction residues in this range (Figure 3). Thermograms for the chemical residues follow a similar pattern to those of MOM, with a small amount of younger but chemically resistant C released at low temperatures, and much older C released in Fmax. As noted above, although the chemical residues contained less than 30% of the total MOM C (Table 1), their thermograms were very similar. The very old Fmax thermal fractions in the chemical residues represent only a small amount (1-4%) of the total bulk soil C (Appendix tables 1 & 2).

3.3 δ^{13}C

The δ^{13}C of CO_2 released from SOM generally increased with temperature in bulk soil and all fractions. The range of δ^{13}C values from F1 to Fmax was the greatest (increasing by 4-5‰) for the chemical residues, and smaller (3-4‰) for the density fractions. Across density fractions, the range of values and the differences in δ^{13}C between different fractions was greater in the deeper soil layer. Interestingly, the FPOM at 30-50 cm was more enriched in ^{13}C than OPOM. At high temperatures subsoil δ^{13}C was generally more enriched than surface soil.

3.4 Contributions of different physical fractions to the thermal oxidation of bulk SOM

Thermograms (Figure 1) demonstrate that C released by the bulk sample at all temperatures contains C contributed from all physical and chemical fractions. For example, of the bulk C released in the temperature range where most C was released (250 to 325°C), FPOM and OPOM contributed 9% and 6%, respectively, of total C released in surface soil, and 16% and 8% in subsoil (Table 1, Fig. 1a). However, at higher temperature ranges, while the total C released was small (<5% of the total C) the proportional contribution from FPOM and OPOM fractions increased to ~40% in surface and 30% in subsoil (Figure 1c).

322   Thus, each thermal fraction from a combusted bulk soil contains C with a broad range of Fm and ^{13}C, with variable contributions from the different physically fractionated components. Figure 5 summarizes the Fm distribution of C

324   across the density and thermal fractions, and emphasizes that the difference of Fm between density fractions (especially FPOM versus MOM) is greater than the range of Fm within any individual density fraction (excluding a

326   small amount of very old MOM) released as a function of temperature or E_a (Figure 5).

328   The measured distribution of ^{14}C for C released with increasing temperature from the bulk soil clearly does not capture the contribution of FPOM with high Fm, because its young C is released across the same temperature ranges

330   as other density and chemical fractions (Figs. 1a, 1c, 3, 4). Thus, the surface soil age distribution misses the ~9% of total C in FPOM that has a much higher ^{14}C signature than bulk soil; instead, its contributions skew the bulk soil

332   thermal ^{14}C (Figure 5, wide bars in the middle of the distribution) higher than the separated MOM thermal fractions (green). This difference is even more pronounced in the subsoil.

334

    With a sufficient number of thermal fractions at high temperatures, thermal analysis of the bulk soil C captured the

336   small percentage of C with very depleted ^{14}C signatures better than the chemical fractions that still mixed younger and older constituents. In surface soil, bulk soil F*max* ^{14}C values (Fm 0.75) were comparable to F*max* fractions of

338   NaF Res. and H_2O_2 Res. (Fm 0.76 and 0.78, respectively), and represented similar amounts of C (2.6%, 2.7%, and 3.0% of total C, respectively) (Appendix table 1). Bulk subsoil F*max* isolated older C (Fm 0.32, 5% of total C) than

340   F*max* values of NaF and H_2O_2 residues (Fm 0.56, 8.1% total C and Fm 0.41, 3.8% total C, respectively), but high-temperature samples were not collected for these fractions because of low C yield (Appendix table 2).

342
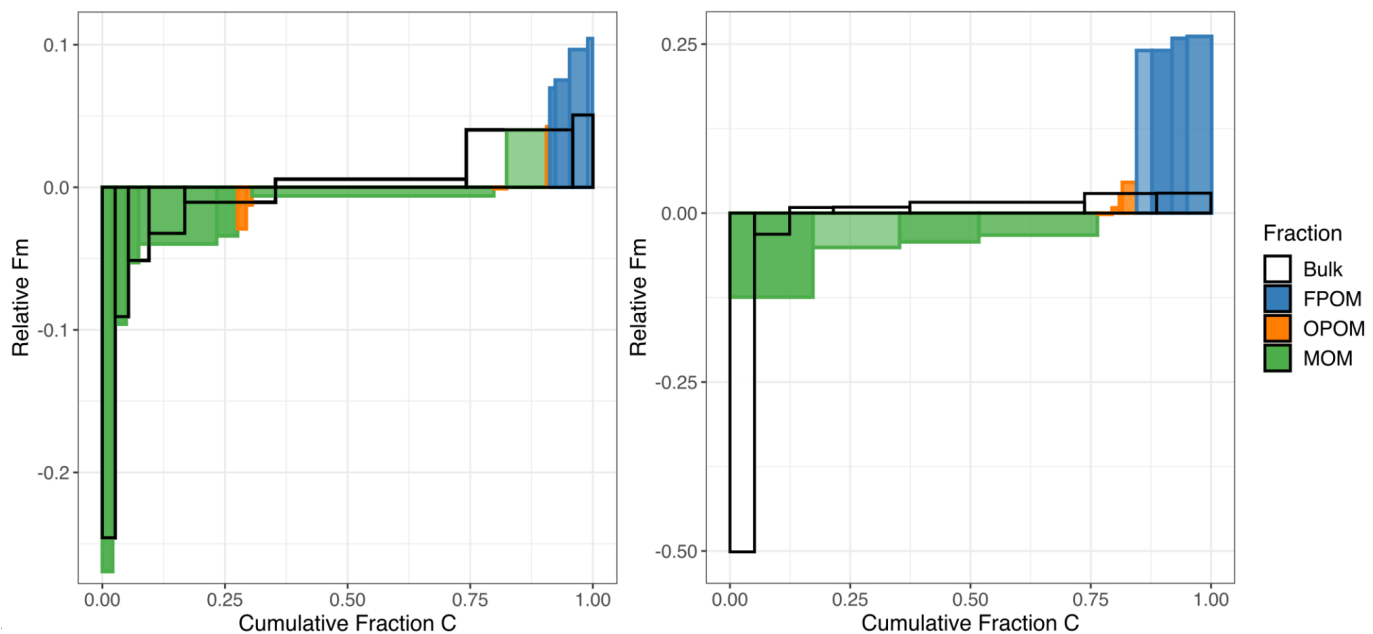
Figure 5: Comparison of the cumulative Fm distribution of C released during thermal fractionation of bulk soil versus oxidation of physically and chemically separated density fractions in the topsoil (left; 0-10cm) and subsoil (right; 30-50cm). The height of each histogram element represents the Fm ^{14}C, normalized to the overall bulk Fm value. Effectively, values above 0 contain more ^{14}C than bulk soil, and values below 0 contain less. The width of bars corresponds to the proportion of total soil C in the fraction. The unfilled histogram elements (no color) represent thermal fractions from the bulk soil, while the colored bars represent the thermally fractionated FPOM, OPOM and MOM fractions shown in previous figures. Darker colors within a fraction correspond to higher temperature / E_a fractions, and lighter colors reflect cooler / lower E_a fractions. Both are ordered by the ^{14}C content, with lowest on the left and highest on the right.

4 Discussion

A main goal of this work is to compare the thermal oxidation profiles and ^{14}C age structures of thermally fractionated SOM with more frequently applied physical (density) and chemical separation methods in a Podzol at two depths. It is critical to find methods to quantify the age distribution of C in SOM, both to relate its persistence to processes operating in soil, and to provide better constraints for testing models of soil C cycling. While density and chemical fractions have proved useful, thermal fractionation offers the advantages of being less expensive and allowing for rapid analysis of the total sample C content. Based on our results, we suggest that separation of FPOM followed by thermal analysis provides the best characterization of the [14]C (age) distribution of C in SOM.

4.1 Activation energy can predict age within a fraction but not between fractions

Thermal fractionation of bulk soils and component physically- and chemically-separated SOM fractions demonstrate that increased thermal stability (i.e., higher E_a) is associated with lower radiocarbon (^{14}C) content (i.e., older C ages;

Fig. 3), and more enriched ^{13}C content (i.e., more microbially processed; Fig. 4). This supports the general assumptions of thermal analysis: that older and more microbially processed/degraded C will be released with increasing temperatures, even among fractions like FPOM that are not associated with minerals (Plante et al., 2009). Because there are large differences in Fm between the physically and chemically separated fractions, C released with similar activation energies (i.e., in a given thermal fraction of bulk soil) therefore can mix C with very different chemistry and ^{14}C age.

For example, particulate fractions FPOM and OPOM that contain fresh plant material as well as microbial residues (Castanha et al., 2008; Angst et al., 2021), release C across a similar temperature range as MOM. While presumably 'labile', FPOM releases C between 300 - 500˚C, reflecting the temperatures required to oxidize molecules like cellulose that make up plant material (Dahiya and Rana, 2004; Plante et al., 2009). Despite a range of activation energies, $\delta^{13}C$ signatures (Fig. 4), and high σE (Table 1) all suggesting chemical diversity, FPOM in this soil is all recent in origin (post-bomb, Fm >1.0) (Fig. 3) and typically breaks down within decades. Because of the temporal dynamics of the bomb spike, an increase or decrease in Fm is more difficult to associate directly to specific age for FPOM, and it is difficult to associate E_a directly to ^{14}C values.

Mineral associated organic matter (MOM) fractions demonstrated larger though mostly overlapping ranges of E_a, but released ^{14}C-depleted and ^{13}C-enriched C above 165 kJ mol^{-1} (Figs. 2 - 4). For most MOM thermal fractions, Fm less than 1.0 reflects the loss of ^{14}C due to radioactive decay and therefore indicates an increase in age. Thus, within a given fraction there are predictable patterns of increasing age and $\delta^{13}C$ with E_a. However, as found in other studies (Leifeld and von Lützow, 2014; Williams et al., 2018; Hemingway et al., 2019), these patterns do not allow prediction of age from E_a alone, highlighting fundamental differences in the processes controlling E_a, ^{14}C content, and age in each fraction. While E_a can either increase or decrease over time as C transforms with decomposition and recycling, the age of the involved C atoms can only increase.

4.2 Age structure of MOM

Both chemical and thermal fractionation methods for MOM indicate the presence of two distinct components with very different Fm, one representing >95% of the C and having Fm similar to that of the bulk MOM but decreasing in ^{14}C with increasing E_a, and a small amount (<5%) of much older C. In this Podzol, the main stabilization mechanisms are likely the interactions between percolating dissolved organic matter and pedogenic (oxy)hydroxides that could explain the large amount of relatively younger C (decades to centuries) removed by NaF and H_2O_2 (Figure 1b) that represents the largest thermal fraction of the MOM (F2). As shown by Schrumpf et al. (2021), the chemical extraction and oxidation of MOM using NaF and H_2O_2, respectively, removed C that was slightly higher in ^{14}C concentration than the MOM overall, leaving smaller but much older residues that resist destabilization. The majority of MOM-C removed through chemical fractionation had similar, younger ages that could reflect SOM more weakly associated with mineral surfaces, while the small proportion remaining could have been trapped within the mineral structure (e.g., in clays on formation) or represent elemental C. Both methods support the idea put forward by

404   Schrumpf et al. (2021) that much of the MOM was cycling on decadal timescales while a small amount (<10%) was much older (Fm 0.628). However, thermal methods demonstrate that the 3% of subsoil MOM oxidized at

406   temperatures greater than 505°C was even older (Fm 0.23, Fig. 3, Table A1).

408   While NaF and H_2O_2 treatments removed younger C, combustion of the residues showed that they still contained C with a range of activation energies and ages. The chemical methods used here are believed to only remove sorbed C

410   that likely has higher Fm (i.e., is younger) than the residue (Kaiser et al., 2007; Mikutta and Kaiser, 2011). These results are somewhat puzzling, as particularly the H_2O_2 treatment is expected to remove all easily oxidizable C,

412   leaving behind C that is either isolated or highly "recalcitrant". We therefore expected that the H_2O_2 residue would not only be older, but also on average have higher E_a. On the contrary, there was actually proportionally less C in

414   F*max* for both residues compared to the unextracted MOM (Figure 1, 3), such that the oldest C in the residues was likely mixed with younger C. The observation that H_2O_2 residues had a range of activation energies and ^{14}C ages

416   could indicate incomplete chemical oxidation or interaction of the OM associated with dissolved pedogenic phases with the remaining mineral phases. Alternatively, the presence of low E_a material with very low ^{14}C could reflect

418   incorporation of sedimentary shale parent material C into microbial food webs with long-term stabilization of microbial residues (Seifert et al., 2013).

420

     Understanding the nature of the small amount of very old C found in MOM and bulk soil, and explaining the age

422   and $\delta^{13}C$ structure of the NaF and H_2O_2 residue thermal fractions, requires additional information. One possibility is that the oldest C persists in the form of charcoal (Cusack et al., 2012; Sanderman et al., 2016) or is derived from

424   the shale parent material of the Wetzstein site (Schrumpf et al., 2011; Grant et al., 2023). Unpublished ^{14}C data collected from the surface of rock fragments found in the soil indicate a Fm of 0.27, similar to values calculated for

426   subsoil MOM F*max* fractions (Table 1). The thermal alteration of sedimentary parent material during metamorphism could also explain the chemical recalcitrance, heavier $\delta^{13}C$, and higher activation energies of this very old C. A

428   second possibility is the presence of non-crystalline minerals that are often correlated with the amount of very old C found in soil (Huang et al., 2016; Khomo et al., 2017; Heckman et al., 2018a). The investigated soils have moderate

430   oxalate extractable Fe contents of 9.2 (0-10 cm) and 17.4 (30-50 cm) g kg^{-1} (Schrumpf et al. 2021 Biogeosciences, supplement). Dithionite extractable Fe concentrations (including both crystalline and non-crystalline components)

432   were 17 and 27.4 g kg^{-1} (respectively). However, quantifying such effects would require investigation of soils with varying amounts of non–crystalline minerals. A third explanation of long SOM persistence is the stochastic nature

434   of the decomposition process. Available C is not uniformly decomposed, and some substrate may persist in soil on much longer timescales (Bolin and Rodhe, 1973; Bosatta and Ågren, 1985; Sierra et al., 2018). Through random

436   chance associated with biological, chemical, and physical processes, a small portion of total SOM remains in soil for centuries to millennia. Such persistent C may be associated with the high activation energies measured here.

438

4.3 Suggested procedure for measuring the ^{14}C distribution of organic C in bulk soils

440 The goal of any fractionation scheme for ^{14}C analysis is to provide clearer delineation of C ages in soil, which integrates multiple types of SOM and stabilization mechanisms. Combining operationally-defined fractionation

442 methods can further isolate distinct pools of C with varying ^{14}C ages. Such age distributions can be used to constrain models of SOM dynamics (Sierra et al., 2014; Metzler et al., 2018; Chanca et al., 2022), and test hypotheses linking

444 stabilization mechanisms with rates of C cycling. Overall, Figure 5 demonstrates that density fractionation alone cannot quantify age structure of bulk SOM, especially of MOM, while thermal fractionation of bulk SOM fails to

446 capture the youngest part of the age distribution. This is because the youngest component of the soil C, the low density FPOM, releases C across nearly the entire range of combustion temperatures (Fig. 1c), making the C released

448 from bulk soil at the lowest temperature reflect ^{14}C ages that are too old, and the C released at higher temperatures too young. At the highest temperatures, however, thermal oxidation methods can isolate C even older than what can

450 be found via aggressive chemical extractions (Fig 3). At the very highest temperatures, the contributions of C from oxidation of FPOM and OPOM are relatively small (Figs. 1c, 2) but may skew data with much younger C.

452

In order to best capture the age distribution of C in SOM, we therefore recommend first separating the low density

454 fraction, then applying thermal fractionation of the heavy fraction with attention to C liberated at very high temperatures to constrain and describe the age structure of MOM. As removal of the FPOM can also be accomplished

456 using size separation, density separation may not be necessary if the main goal is to remove relatively fresh plant material (Castanha et al., 2008; Lavallee et al., 2020). However, the presence of charcoal that would be removed by

458 density but not size could complicate the interpretation of thermal fractions, and further work is needed to resolve this special circumstance.

460

Describing the distribution of ages in SOM is a powerful tool for testing hypotheses about the timescales of different

462 C stabilization mechanisms in soils, and for comparison with age distributions produced by multi-compartment models (Metzler et al., 2018; Chanca et al., 2022). Our results are for a single soil, a Podzol that likely has one major

464 mechanism for stabilizing C on mineral surfaces: interaction with pedogenic oxides. To explore other mineral stabilization mechanisms and timescales, it would be useful to compare thermograms and age distributions for soils

466 with different mineral composition - e.g., allophane, 2:1 clays, 1:1 clays, sands, and as well as mixed mineralogy soils. Additionally, comparison with temperature-resolved spectra (e.g., py-GC/MS, (Sanderman and Grandy, 2020),

468 DRIFTS (Nkwain et al., 2018), etc.) that associate SOM chemistry with thermal stability may help to determine the roles that OM chemistry and mineralogy play in controlling C age and persistence in soil.

470

5 Conclusions

472 Each density and chemical fraction contained a spectrum of SOM ages. FPOM and OPOM displayed more homogeneous ages, while the MOM fraction displayed two distinct age components in this Podzol, identified in both

474 top- and subsoil: likely the younger component that represents the majority of MOM stabilized by association with pedogenic (oxy)hydroxides, and the much older component possibly inherited from shale parent material.

We conclude that thermal fractionation cannot completely replace standard fractionation methods to connect SOM properties (e.g., activation energy) to age distributions. Fresh FPOM contributes young C of homogenous age across temperatures up to 550˚C and thus dilutes the signal of older C from other fractions. This method was effective at identifying multiple stabilization timescales on the MOM fraction, suggesting complex dynamics that may react across multiple timescales including those relevant to climate and management change. We thus recommend separating and measuring ^{14}C of FPOM, then analyzing thermal fractions of MOM to help distinguish faster- and slower-cycling mineral associated components. This additional fractionation helps to go beyond using mean ^{14}C values towards characterizing ^{14}C distributions that can provide a more comprehensive description of SOM cycling and potentially a more stringent test for models. Further efforts are needed to explore the effects of diverse mineral stabilization mechanisms on thermograms and ^{14}C distributions of MOM fractions.

Data Availability

Available via DOI 10.5281/zenodo.7998659

Acknowledgments

This work was funded by the European Research Council (Horizon 2020 Research and Innovation Program; grant no. 695101; 14Constraint) and the Max Planck Society. We gratefully acknowledge our reviewers who helped improve the manuscript. We thank Dr. Axel Steinhof and Dr. Xiaomei Xu for their invaluable assistance in developing the equipment and methods used in this study. We also thank the staff of the Max Planck Institute for Biogeochemistry, UC Irvine, and the Woods Hole Oceanographic Institute for their assistance in radiocarbon sampling and data preparation. Finally, we thank the CarboEurope Project for access to the archived soils used in this study.

Author Contributions

SWS and ST designed, constructed, and tested method hardware and protocols. Data were collected by SWS and analyzed by SWS and MS with input from all authors. SWS led the writing of the manuscript with significant contribution from ST and input from all authors.

6 References

Anderson, D. W. and Paul, E. A.: Organo-Mineral Complexes and Their Study by Radiocarbon Dating, Soil Science Society of America Journal, 48, 298–301, https://doi.org/10.2136/sssaj1984.03615995004800020014x, 1984.

Angst, G., Mueller, K. E., Nierop, K. G. J., and Simpson, M. J.: Plant- or microbial-derived? A review on the molecular composition of stabilized soil organic matter, Soil Biol Biochem, 156, 108189, https://doi.org/10.1016/j.soilbio.2021.108189, 2021.

Baisden, W. T. and Canessa, S.: Using 50 years of soil radiocarbon data to identify optimal approaches for estimating soil carbon residence times, Nucl Instrum Methods Phys Res B, 294, 588–592, https://doi.org/10.1016/j.nimb.2012.06.021, 2013.

Balesdent, J.: The turnover of soil organic fractions estimated by radiocarbon dating, Science of the Total Environment, The, 62, 405–408, https://doi.org/10.1016/0048-9697(87)90528-6, 1987.

Basile-Doelsch, I., Balesdent, J., and Pellerin, S.: Reviews and syntheses: The mechanisms underlying carbon storage in soil, Biogeosciences, 17, 5223–5242, https://doi.org/10.5194/bg-17-5223-2020, 2020.

Bianchi, T. S., Galy, V., Rosenheim, B. E., Shields, M., Cui, X., and Van Metre, P.: Paleoreconstruction of organic carbon inputs to an oxbow lake in the Mississippi River watershed: Effects of dam construction and land use change on regional inputs, Geophys Res Lett, 42, 7983–7991, https://doi.org/10.1002/2015GL065595, 2015.

Bolin, B. and Rodhe, H.: A note on the concepts of age distribution and transit time in natural reservoirs, Tellus, 25, 58–62, https://doi.org/10.1111/j.2153-3490.1973.tb01594.x, 1973.

Bosatta, E. and Ågren, G. I.: Theoretical analysis of decomposition of heterogeneous substrates, Soil Biol Biochem, 17, 601–610, https://doi.org/10.1016/0038-0717(85)90035-5, 1985.

Castanha, C., Trumbore, S., and Amundson, R.: Methods of separating soil carbon pools affect the chemistry and turnover time of isolated fractions, Radiocarbon, 50, 83–97, https://doi.org/10.1017/S0033822200043381, 2008.

Chanca, I., Trumbore, S., Macario, K., and Sierra, C. A.: Probability Distributions of Radiocarbon in Open Linear Compartmental Systems at Steady-State, J Geophys Res Biogeosci, 127, 1–23, https://doi.org/10.1029/2021JG006673, 2022.

De Coninck, F.: Major mechanisms in formation of spodic horizons, Geoderma, 24, 101–128, 1980.

Cotrufo, M. F., Ranalli, M. G., Haddix, M. L., Six, J., and Lugato, E.: Soil carbon storage informed by particulate and mineral-associated organic matter, Nat Geosci, 12, 989–994, https://doi.org/10.1038/s41561-019-0484-6, 2019.

Cusack, D. F., Chadwick, O. A., Hockaday, W. C., and Vitousek, P. M.: Mineralogical controls on soil black carbon preservation, Global Biogeochem Cycles, 26, 1–10, https://doi.org/10.1029/2011GB004109, 2012.

Dahiya, J. B. and Rana, S.: Thermal degradation and morphological studies on cotton cellulose modified with various arylphosphorodichloridites, Polym Int, 53, 995–1002, https://doi.org/10.1002/pi.1500, 2004.

Feng, X. and Simpson, M. J.: Temperature responses of individual soil organic matter components, J Geophys Res Biogeosci, 113, 1–14, https://doi.org/10.1029/2008JG000743, 2008.

González-Pérez, J. A., Chabbi, A., de la Rosa, J. M., Rumpel, C., and González-Vila, F. J.: Evolution of organic matter in lignite-containing sediments revealed by analytical pyrolysis (Py-GC-MS), Org Geochem, 53, 119–130, https://doi.org/10.1016/j.orggeochem.2012.08.001, 2012.

Grandy, A. S., Strickland, M. S., Lauber, C. L., Bradford, M. A., and Fierer, N.: The influence of microbial communities, management, and soil texture on soil organic matter chemistry, Geoderma, 150, 278–286, https://doi.org/10.1016/j.geoderma.2009.02.007, 2009.

Grant, K. E., Galy, V. V., Chadwick, O. A., and Derry, L. A.: Thermal oxidation of carbon in organic matter rich volcanic soils: insights into SOC age differentiation and mineral stabilization, Biogeochemistry, 144, 291–304, https://doi.org/10.1007/s10533-019-00586-1, 2019.

Grant, K. E., Hilton, R. G., and Galy, V.: Global patterns of radiocarbon depletion in subsoil linked to rock-derived organic carbon, Geochem Perspect Lett, 36–40, 2023.

550   Gregorich, E. G., Beare, M. H., McKim, U. F., and Skjemstad, J. O.: Chemical and Biological Characteristics of Physically Uncomplexed Organic Matter, Soil Science Society of America Journal, 70, 975–985,

552   https://doi.org/10.2136/sssaj2005.0116, 2006.

Heckman, K., Lawrence, C. R., and Harden, J. W.: A sequential selective dissolution method to quantify storage and

554   stability of organic carbon associated with Al and Fe hydroxide phases, Geoderma, 312, 24–35, https://doi.org/10.1016/j.geoderma.2017.09.043, 2018a.

556   Heckman, K., Throckmorton, H., Horwath, W., Swanston, C., and Rasmussen, C.: Variation in the Molecular Structure and Radiocarbon Abundance of Mineral-Associated Organic Matter across a Lithosequence of Forest

558   Soils, Soil Syst, 2, 36, https://doi.org/10.3390/soilsystems2020036, 2018b.

Heckman, K., Hicks Pries, C. E., Lawrence, C. R., Rasmussen, C., Crow, S. E., Hoyt, A. M., von Fromm, S. F., Shi,

560   Z., Stoner, S., McGrath, C., Beem-Miller, J., Berhe, A. A., Blankinship, J. C., Keiluweit, M., Marín-Spiotta, E., Monroe, J. G., Plante, A. F., Schimel, J., Sierra, C. A., Thompson, A., and Wagai, R.: Beyond bulk: Density

562   fractions explain heterogeneity in global soil carbon abundance and persistence, Glob Chang Biol, 28, 1178–1196, https://doi.org/10.1111/gcb.16023, 2022.

564   Helfrich, M., Flessa, H., Mikutta, R., Dreves, A., and Ludwig, B.: Comparison of chemical fractionation methods for isolating stable soil organic carbon pools, Eur J Soil Sci, 58, 1316–1329, https://doi.org/10.1111/j.1365-

566   2389.2007.00926.x, 2007.

Hemingway, J. D.: rampedpyrox: Open-source tools for thermoanalytical data analysis, 2016, 2017.

568   Hemingway, J. D., Rothman, D. H., Rosengard, S. Z., and Galy, V. V.: Technical note: An inverse method to relate organic carbon reactivity to isotope composition from serial oxidation, Biogeosciences, 14, 5099–5114,

570   https://doi.org/10.5194/bg-14-5099-2017, 2017.

Hemingway, J. D., Rothman, D. H., Grant, K. E., Rosengard, S. Z., Eglinton, T. I., Derry, L. A., and Galy, V. V.:

572   Mineral protection regulates long-term global preservation of natural organic carbon, Nature, 570, 228–231, https://doi.org/10.1038/s41586-019-1280-6, 2019.

574   Huang, X., Jiang, H., Li, Y., Ma, Y., Tang, H., Ran, W., and Shen, Q.: The role of poorly crystalline iron oxides in the stability of soil aggregate-associated organic carbon in a rice-wheat cropping system, Geoderma, 279, 1–10,

576   https://doi.org/10.1016/j.geoderma.2016.05.011, 2016.

Jagadamma, S., Lal, R., Ussiri, D. A. N., Trumbore, S. E., and Mestelan, S.: Evaluation of structural chemistry and

578   isotopic signatures of refractory soil organic carbon fraction isolated by wet oxidation methods, Biogeochemistry, 98, 29–44, https://doi.org/10.1007/s10533-009-9374-0, 2010.

580   Kaiser, K., Mikutta, R., and Guggenberger, G.: Increased Stability of Organic Matter Sorbed to Ferrihydrite and Goethite on Aging, Soil Science Society of America Journal, 71, 711–719,

582   https://doi.org/10.2136/sssaj2006.0189, 2007.

Khomo, L., Trumbore, S., Bern, C. R., and Chadwick, O. A.: Timescales of carbon turnover in soils with mixed

584   crystalline mineralogies, Soil, 3, 17–30, https://doi.org/10.5194/soil-3-17-2017, 2017.

Kleber, M., Bourg, I. C., Coward, E. K., Hansel, C. M., Myneni, S. C. B., and Nunan, N.: Dynamic interactions at

586   the mineral–organic matter interface, Nat Rev Earth Environ, 0123456789, https://doi.org/10.1038/s43017-021-00162-y, 2021.

588   Lavallee, J. M., Soong, J. L., and Cotrufo, M. F.: Conceptualizing soil organic matter into particulate and mineral-associated forms to address global change in the 21st century, Glob Chang Biol, 26, 261–273,

590   https://doi.org/10.1111/gcb.14859, 2020.

Lehmann, J. and Kleber, M.: The contentious nature of soil organic matter, Nature, 528, 60–68,

592   https://doi.org/10.1038/nature16069, 2015.

Leifeld, J. and von Lützow, M.: Chemical and microbial activation energies of soil organic matter decomposition,

594   Biol Fertil Soils, 50, 147–153, https://doi.org/10.1007/s00374-013-0822-6, 2014.

von Lützow, M., Kögel-Knabner, I., Ekschmitt, K., Flessa, H., Guggenberger, G., Matzner, E., and Marschner, B.:

596   SOM fractionation methods: Relevance to functional pools and to stabilization mechanisms, Soil Biol Biochem, 39, 2183–2207, https://doi.org/10.1016/j.soilbio.2007.03.007, 2007.

598   Metzler, H., Müller, M., and Sierra, C. A.: Transit-time and age distributions for nonlinear time-dependent
compartmental systems, Proc Natl Acad Sci U S A, 115, 1150–1155, https://doi.org/10.1073/pnas.1705296115,
600   2018.

Mikutta, R. and Kaiser, K.: Organic matter bound to mineral surfaces: Resistance to chemical and biological
602   oxidation, Soil Biol Biochem, 43, 1738–1741, https://doi.org/10.1016/j.soilbio.2011.04.012, 2011.

Natali, C., Bianchini, G., and Carlino, P.: Thermal stability of soil carbon pools: Inferences on soil nature and
604   evolution, Thermochim Acta, 683, 178478, https://doi.org/https://doi.org/10.1016/j.tca.2019.178478, 2020.

Nkwain, F. N., Demyan, M. S., Rasche, F., Dignac, M. F., Schulz, E., Kätterer, T., Müller, T., and Cadisch, G.:
606   Coupling pyrolysis with mid-infrared spectroscopy (Py-MIRS) to fingerprint soil organic matter bulk chemistry,
J Anal Appl Pyrolysis, 133, 176–184, https://doi.org/10.1016/j.jaap.2018.04.004, 2018.

Paul, E. A., Follett, R. F., Leavitt, S. W., Halvorson, A., Peterson, G. A., and Lyon, D. J.: Radiocarbon Dating for
608   Determination of Soil Organic Matter Pool Sizes and Dynamics, Soil Science Society of America Journal, 61,
610   1058–1067, https://doi.org/10.2136/sssaj1997.03615995006100040011x, 1997.

Plante, A. F., Fernández, J. M., and Leifeld, J.: Application of thermal analysis techniques in soil science,
612   Geoderma, 153, 1–10, https://doi.org/10.1016/j.geoderma.2009.08.016, 2009.

Plante, A. F., Fernández, J. M., Haddix, M. L., Steinweg, J. M., and Conant, R. T.: Biological, chemical and thermal
614   indices of soil organic matter stability in four grassland soils, Soil Biol Biochem, 43, 1051–1058,
https://doi.org/10.1016/j.soilbio.2011.01.024, 2011.

Plante, A. F., Beaupré, S. R., Roberts, M. L., and Baisden, T.: Distribution of Radiocarbon Ages in Soil Organic
616   Matter by Thermal Fractionation, Radiocarbon, 55, 1077–1083, https://doi.org/10.1017/s0033822200058215,
618   2013.

Quénéa, K., Derenne, S., González-Vila, F. J., González-Pérez, J. A., Mariotti, A., and Largeau, C.: Double-shot
620   pyrolysis of the non-hydrolysable organic fraction isolated from a sandy forest soil (Landes de Gascogne,
South-West France): Comparison with classical Curie point pyrolysis, J Anal Appl Pyrolysis, 76, 271–279,
622   https://doi.org/10.1016/j.jaap.2005.12.007, 2006.

Rasmussen, C., Throckmorton, H., Liles, G., Heckman, K., Meding, S., and Horwath, W. R.: Controls on soil
624   organic carbon partitioning and stabilization in the California Sierra Nevada, Soil Syst, 2, 1–18,
https://doi.org/10.3390/soilsystems2030041, 2018.

Rennert, T. and Herrmann, L.: Sea spray and land use effects on clay minerals and organic matter of soils on
626   machair (Harris, Scotland), Geoderma Regional, 23, e00339, https://doi.org/10.1016/j.geodrs.2020.e00339,
628   2020.

Rennert, T. and Herrmann, L.: Thermal-gradient analysis of soil organic matter using an elemental analyser – A tool
630   for qualitative characterization?, Geoderma, 425, 116085, https://doi.org/10.1016/j.geoderma.2022.116085,
2022.

Rosenheim, B. E. and Galy, V.: Direct measurement of riverine particulate organic carbon age structure, Geophys
632   Res Lett, 39, 1–6, https://doi.org/10.1029/2012GL052883, 2012.

Rosenheim, B. E., Day, M. B., Domack, E., Schrum, H., Benthien, A., and Hayes, J. M.: Antarctic sediment
634   chronology by programmed-temperature pyrolysis: Methodology and data treatment, Geochemistry,
636   Geophysics, Geosystems, 9, 1–16, https://doi.org/10.1029/2007GC001816, 2008.

Sanderman, J. and Grandy, S. A.: Ramped thermal analysis for isolating biologically meaningful soil organic matter
638   fractions with distinct residence times, Soil, 6, 131–144, https://doi.org/10.5194/soil-6-131-2020, 2020.

Sanderman, J., Baisden, W. T., and Fallon, S.: Redefining the inert organic carbon pool, Soil Biol Biochem, 92,
640   149–152, https://doi.org/10.1016/j.soilbio.2015.10.005, 2016.

Schrumpf, M., Schulze, E. D., Kaiser, K., and Schumacher, J.: How accurately can soil organic carbon stocks and
642   stock changes be quantified by soil inventories?, Biogeosciences, 8, 1193–1212, https://doi.org/10.5194/bg-8-
1193-2011, 2011.

Schrumpf, M., Kaiser, K., Guggenberger, G., Persson, T., Kögel-Knabner, I., and Schulze, E. D.: Storage and
644   stability of organic carbon in soils as related to depth, occlusion within aggregates, and attachment to minerals,
646   Biogeosciences, 10, 1675–1691, https://doi.org/10.5194/bg-10-1675-2013, 2013.

648 Schrumpf, M., Kaiser, K., Mayer, A., Hempel, G., and Trumbore, S.: Age distribution, extractability, and stability of mineral-bound organic carbon in central European soils, Biogeosciences, 18, 1241–1257, https://doi.org/10.5194/bg-18-1241-2021, 2021.

650 Schuur, E. A. G., Trumbore, S. E., and Druffel, E. R. M.: Radiocarbon and Climate Change: Mechanisms, Applications and Laboratory Techniques, 1–315 pp., https://doi.org/10.1007/978-3-319-25643-6, 2016.

652 Seifert, A. G., Trumbore, S., Xu, X., Zhang, D., and Gleixner, G.: Variable effects of plant colonization on black slate uptake into microbial PLFAs, Geochim Cosmochim Acta, 106, 391–403, 654 https://doi.org/10.1016/j.gca.2012.12.011, 2013.

Sierra, C. A., Müller, M., and Trumbore, S. E.: Modeling radiocarbon dynamics in soils: SoilR version 1.1, Geosci 656 Model Dev, 7, 1919–1931, https://doi.org/10.5194/gmd-7-1919-2014, 2014.

Sierra, C. A., Hoyt, A. M., He, Y., and Trumbore, S. E.: Soil Organic Matter Persistence as a Stochastic Process: 658 Age and Transit Time Distributions of Carbon in Soils, Global Biogeochem Cycles, 32, 1574–1588, https://doi.org/10.1029/2018GB005950, 2018.

660 Sollins, P., Kramer, M. G., Swanston, C., Lajtha, K., Filley, T., Aufdenkampe, A. K., Wagai, R., and Bowden, R. D.: Sequential density fractionation across soils of contrasting mineralogy: Evidence for both microbial- and 662 mineral-controlled soil organic matter stabilization, Biogeochemistry, 96, 209–231, https://doi.org/10.1007/s10533-009-9359-z, 2009.

664 Torn, M. S., Trumbore, S. E., Chadwick, O. A., Vitousek, P. M., and Hendricks, D. M.: Mineral control of soil organic carbon and storage and turnover, Nature, 389, 3601–3603, 1997.

666 Trumbore, S.: Age of soil organic matter and soil respiration: Radiocarbon constraints on belowground C dynamics, Ecological Applications, 10, 399–411, https://doi.org/10.1890/1051-0761(2000)010[0399:AOSOMA]2.0.CO;2, 668 2000.

Trumbore, S. E.: Comparisons of carbon dynamics in tropical and temperate soils using radiocarbon measurements, 670 Measurement, 7, 275–290, 1993.

Trumbore, S. E. and Zheng, S.: Comparison of fractionation methods for soil organic matter 14C analysis, 38, 219– 672 229, 1996.

Trumbore, S. E., Bonani, G., and Wolfli, W.: The rates of carbon cycling in several soils from AMS14C 674 measurements of fractionated soil organic matter, John Wiley and Sons Inc, United States, 1990.

Wendeberg, M., Richter, J. M., Rothe, M., and Brand, W. A.: Jena Reference Air Set (JRAS): A multi-point scale 676 anchor for isotope measurements of CO2in air, Atmos Meas Tech, 6, 817–822, https://doi.org/10.5194/amt-6-817-2013, 2013.

678 Williams, E. K., Fogel, M. L., Berhe, A. A., and Plante, A. F.: Distinct bioenergetic signatures in particulate versus mineral-associated soil organic matter, Geoderma, 330, 107–116, 680 https://doi.org/10.1016/j.geoderma.2018.05.024, 2018.

Xu, X., Trumbore, S. E., Zheng, S., Southon, J. R., McDuffee, K. E., Luttgen, M., and Liu, J. C.: Modifying a sealed 682 tube zinc reduction method for preparation of AMS graphite targets: Reducing background and attaining high precision, Nucl Instrum Methods Phys Res B, 259, 320–329, https://doi.org/10.1016/j.nimb.2007.01.175, 2007.

684

686 Stoner, Shane et al.: Datasets and code for this publication, https://doi.org/10.5281/zenodo.7998659, 2023.